Journal of The Electrochemical Society, 2021 **168** 014512

The Discrepancy in Oxygen Evolution Reaction Catalyst Lifetime Explained: RDE vs MEA - Dynamicity within the Catalyst Layer Matters

Mohammad Fathi Tovini,[=] Alexandra Hartig-Weiß,[=,*] Hubert A. Gasteiger,[**] and Hany A. El-Sayed[z]

Chair of Technical Electrochemistry, Department of Chemistry and Catalysis Research Center, Technical University of Munich, 85748 Garching, Germany

This study reveals the source of discrepancy between the lifetime of oxygen evolution reaction (OER) catalysts determined by rotating disk electrode (RDE) measurements vs that obtained in a membrane electrode assembly (MEA) in an electrolyzer. We show that the accumulation of microscopic oxygen bubbles in the pores of the electro-catalyst layer during the OER takes place in both RDE and MEA measurements. However, this accumulation was found to be much more significant in RDE measurements, where the shielding of almost all of the catalyst active sites by gas bubbles leads to rapid performance deterioration. This decrease in performance, albeit largely reversible, was found to also induce irreversible catalyst degradation, which could be avoided if the accumulation of microscopic bubbles is prevented. This type of artefact results in vastly under-estimated catalyst lifetimes obtained by RDE experiments, resulting in values that are orders of magnitude shorter than those obtained using MEA measurements, and a hypothesis for this discrepancy will be proposed. Therefore, electrochemical cells with liquid electrolytes are not reliable for OER catalyst lifetime determination.

This was paper 236 presented at the Atlanta, Georgia, Meeting of the Society, October 13–17, 2019.

 [DOI: 10.1149/1945-7111/abdcc9]

Manuscript submitted October 22, 2020; revised manuscript received December 21, 2020. Published January 29, 2021. *This paper is part of the JES Focus Issue on Proton Exchange Membrane Fuel Cell and Proton Exchange Membrane Water Electrolyzer Durability.*

Supplementary material for this article is available online

The slow kinetics of the oxygen evolution reaction (OER) is a major challenge in the electrochemical production of hydrogen from water by proton exchange membrane water electrolysis (PEM-WE). To date, IrO_2 and RuO_2 are the most investigated catalysts in the literature for OER catalysis.[1–3] In order to identify a suitable OER catalyst, its activity and long-term stability are of an equally critical importance. Reliable methods for screening the activity have been established using rotating disk electrode (RDE) and flow-channel techniques or testing membrane electrode assemblies (MEAs) in PEM-WEs.[4–10] However, the evaluation of the long-term stability of OER catalysts under realistic conditions is not feasible due to the rather low degradation rate in PEM-WEs, which would require 1000's of hours of testing to obtain significant degradation.[11,12] Therefore, accelerated degradation tests are required, which are typically performed in cells with liquid electrolyte or in PEM-WEs.[12–17] Generally, accelerated degradation tests are performed using one or more of three different methods: i) constant current holds (chronopotentiometry), ii) constant potential holds (chronoamperometry), and iii) potential cycling.[18]

Applying a constant current is the prevalent testing method in the literature.[19] In this method, which is carried out in an RDE setup, the increase in OER overpotential at constant current operation is taken as a measure for catalyst stability, where a drastic potential jump is interpreted as the end of life (EOL) of the catalyst.[15,20–22] Alternatively, constant potential and potential cycling methods are also utilized to perform accelerated degradation tests in which the deterioration of current as a function of time or cycle number is taken as representative of catalyst stability.[8,23–29]

It is well established now that there is a discrepancy between a catalyst lifetime obtained from RDE and PEM-WE under similar operating conditions.[14,30,31] The extremely short lifetime of a catalyst obtained from RDE testing using the constant current method and indicated by the sudden potential jump was attributed to the disk electrode substrate passivation, making the catalyst no longer electrochemically accessible due to the high contact resistance.[11] On the other hand, Tan et al. evaluated a variety of Ir-based catalysts and showed that the phase transformation of the active sites from the highly OER-active hydrous Ir oxy-hydroxide to the less OER-active anhydrous-IrO_x exerts a harsher oxidative condition (higher potentials) on the electrode.[32]

The OER catalyst performance loss during RDE based stability measurements can, at least in part, be ascribed to the passivation of the RDE disk material, to the dissolution and/ or the physical detachment of the OER catalyst (as evidenced by the quantification of dissolved Ir after RDE tests),[32] and to the accumulation of microscopic oxygen bubbles within the catalyst layer. In our recent studies, we discovered the effect of the latter on the stability results obtained from RDE experiments.[31,33] We have shown that the accumulation of microscopic oxygen bubbles in the pores of a catalyst layer during constant current electrolysis in RDE measurements is causing the apparent catalyst deactivation and failure.[31] The effect of such microscopic bubbles on the performance loss of a catalyst during a gas-evolving reaction was further proven by subjecting the electrochemical cell or the electrolyte to ultrasonication while conducting a typical RDE-based measurement.[33,34]

In this study, we demonstrate that the accumulation of microscopic oxygen bubbles in the catalyst layer strongly affects the outcome of RDE based durability tests, independent of whether they are based on constant current, constant potential, or potential cycling methods. In addition, we show that the same phenomenon leads to a decay of OER catalyst activity in PEM water electrolyzer based aging tests, in which case, however, the OER activity loss can be fully recovered, even after 100's of hours. We also provide an explanation as to why the accumulation of microscopic oxygen bubbles in the catalyst layer is detrimental in RDE testing, while in MEA based tests in an electrolyzer it only causes reversible degradation processes that are fully recoverable.

[=]These authors contributed equally to this work.
*Electrochemical Society Student Member.
**Electrochemical Society Fellow.
[z]E-mail: hany.el-sayed@tum.de

Experimental

Rotating disk electrode (RDE).—Electrochemical measurements were carried out in a water jacketed three-electrode cell using a reversible hydrogen electrode (RHE) as a reference electrode, a high surface area Au wire as a counter electrode and a rotating ring-disk electrode (RRDE) consisting of a 5 mm diameter polycrystalline Au disk and Pt ring supported by PTFE body (Pine Research Instrumentation, USA) as a working electrode. The reference electrode potential was calibrated in a H_2-saturated electrolyte prior to each experiment using the Pt ring of the RRDE.

A 0.05 M H_2SO_4 aqueous solution was used as electrolyte, which was prepared by mixing high purity H_2SO_4 (Ultrapur, 96%, Merck Millipore KGaA, Germany) and ultra-pure water (18.2 MΩ cm at 20 °C, Merck Millipore KGaA, Germany). High purity Ar and H_2 (6.0-grade, Westfalen AG) were used to purge the electrolyte.

All RDE electrochemical measurements were performed using an Autolab potentiostat (PGSTAT302N, Metrohm AG) and a rotator (Pine Research Instrumentation) with a polyether ketone shaft. The electrode rotation rate was fixed at 2500 RPM and the electrolyte temperature was maintained at 40 °C using the water jacket. Freshly coated electrodes were dipped in Ar-saturated electrolyte and the non-compensated solution resistance between the reference and working electrode was determined by electrochemical impedance spectroscopy (EIS) from 100 kHz to 100 Hz at open circuit potential (OCP). Then, cyclic voltammetry (CV) was performed between 0.05–1.25 V vs RHE with 20 mVs^{-1} scan rate for 10 cycles. Afterwards, the OER polarization curve was recorded between 1.2–1.55 V vs RHE at 10 mVs^{-1}. The catalyst OER stability tests were performed by the constant current, constant potential and potential cycling methods in Ar-saturated electrolyte. The initial 100 ms of the constant current and constant potential measurements were excluded in the final graphs in order to eliminate the capacitive contributions to the OER current. This time approximately corresponds to five times the time constant (RC) of the RDE configuration, as calculated by EIS results (not shown here). Due to decay of the current during the constant potential stability measurements, an online iR compensation was utilized in order to apply a constant iR-free potential of 1.53 V_{RHE} to the electrode according to the following equation:

$$E_{iR-free} = E_{measured} - i_{OER} \times R$$

where R is the high frequency resistance measured by EIS prior to each measurement.

Before each measurement, the Au working electrode was polished with 0.3 μm alumina polishing suspension (Buhler AG) and sonicated in ultrapure water for several times. The catalyst ink suspension was prepared using 10.46 mg of IrO_2 supported on TiO_2 (IrO_2/TiO_2 with 75 wt.% iridium, Elyst Ir75 0480 from Umicore, Germany), 2 ml ultrapure water, and 2.4 μl Nafion® ionomer solution (5 wt.% ionomer, Sigma Aldrich) in order to achieve ≈1 wt.% ionomer content in the final coating. The suspension was sonicated for 30 min in a sonication bath (Elmasonic S 30 H, Elma Schmidbauer GmbH) in order to achieve a homogenous ink. The temperature of the bath was maintained below 35 °C in order to prevent solvent evaporation. Finally, 20 μl of the prepared ink was drop-casted on the cleaned Au working electrode in order to achieve an iridium loading of 0.4 $mg_{Ir}\ cm^{-2}{}_{disk}$. Since RDE is known to be a thin-film technique with controlled mass-transport, high loadings and thus, thick catalyst layers, should be avoided.[35] Due to the rather high packing density of the IrO_2/TiO_2 catalyst (≈2.3 $g_{Ir}cm^{-3}$),[36] a loading of 0.4 $mg_{Ir}\ cm^{-2}{}_{disk}$ already results in a ≈1.7 μm thick catalyst layer. Since this is already quite thick, a higher loading was not feasible within the RDE setup.

Membrane electrode assembly (MEA) preparation and cell assembly.—Using the decal transfer method, MEAs with an active area of 5 cm^2 were prepared. Platinum supported on Vulcan XC72 carbon (45.8 wt.% Pt/C, TEC10V50E from Tanaka, Japan) was used as a hydrogen evolution reaction (HER) catalyst on the cathode electrode and IrO_2 supported on TiO_2 (same as above) as an OER catalyst on the anode electrode. The inks were prepared by mixing de-ionized (DI) water (18 MΩ cm), 2-propanol (purity ⩾ 99.9% from Sigma Aldrich) and Nafion® ionomer solution (20 wt.% ionomer, D2021 from IonPower, USA) together with the respective amount of catalyst. After mixing the suspension for 24 h using a roller mixer, where ZrO_2 grinding balls (5 mm diameter) were added to achieve a homogenous suspension, the ink was coated onto a thin plastic foil (PTFE, 50 μm thick, from Angst + Pfister, Germany) using the Mayer rod technique. After drying, 5 cm^2 decals were cut from the coating and hot-pressed onto a Nafion® 212 membrane (50 μm thick, from Quintech, Germany) at 155 °C for 3 min at a pressure of 2.5 MPa. The actual weight of the decals was determined by weighing the decals before and after the hot-pressing. Throughout the study, the loading was kept constant at 0.3 ± 0.1 $mg_{Pt}\ cm^{-2}{}_{MEA}$ for the hydrogen cathode and 1.9 ± 0.2 $mg_{Ir}\ cm^{-2}{}_{MEA}$ for the oxygen anode, respectively. Since low loadings (<0.6 $mg_{Ir}cm^{-2}{}_{geo}$) lead to additional performance losses due to an inhomogeneous catalyst [37] and in order to be more representative of state-of-the-art loadings (≈2.3 $g_{Ir}cm^{-3}$),[38] a rather high loading compared to the RDE setup was chosen for the MEA configuration. The ionomer content was ∼11 wt.%. Sintered titanium (from Mott Corporation, USA) with a porosity of ≈50% and a thickness of 280 ± 10 μm was used as a porous transport layer (PTL) on the anode, whereas on the cathode, a carbon fiber paper (TGP-H 120 T from Toray, no MPL, 20 wt.% PTFE) with a thickness of 370 ± 10 μm was used. The MEA and the PTLs were placed between the flow fields of the electrolyzer cell, and additional virginal PTFE sheets were used as gaskets. A compression of 25% for the carbon PTL was achieved by choosing the right thickness of the gaskets. Specific details about the cell hardware are reported elsewhere.[39]

Electrochemical characterization of MEAs.—An automated test station from Greenlight Innovation was used to perform all the electrochemical measurements of the MEAs. Throughout the whole test, the anode was supplied with 5 ml min^{-1} deionized (DI) water, which was pre-heated to 80 °C for the MEA conditioning procedure and to 40 °C before the stability measurements. During the stability measurements, the cell temperature was kept constant at 40 °C and the produced gas on the anode side was diluted with nitrogen (100 nccm) to avoid the formation of an explosive gas mixture due to hydrogen permeation through the membrane into the anode compartment. Initially, the cell was conditioned at 1 A cm^{-2} for 30 min at 80 °C under nitrogen atmosphere. Subsequently, three consecutive polarization curves were taken at ambient pressure (1 bar_a) and 80 °C, by increasing the current density from 0.01 to 4 A cm^{-2} stepwise and holding at each current for 5 min to ensure a stable cell voltage. The last 10 s of the cell voltage at each current density were averaged. Considering these polarization curves as part of the conditioning, they were not included in the analysis. Subsequently, another polarization curve was recorded at 40 °C, which was used as a reference (beginning of test, BOT). Additionally, AC impedance measurements were performed at each current density in a range from 100 kHz to 1 Hz. The amplitude of the current perturbation was adjusted for each step individually in order to fulfill the criteria of linearity, while still maintaining a sufficient signal to noise ratio. The high-frequency intercept with the real axis in a Nyquist plot was used to determine the high frequency resistance (HFR). At the beginning of test (BoT) as well as at the end of test (EoT), cyclic voltammograms (CVs) of the anode electrode were recorded by flushing the cathode counter electrode with dry H_2 (50 ml min^{-1}) to ensure a stable reference potential and supplying the anode electrode with DI water (5 ml min^{-1}). The CVs were recorded in a potential range of 0.05 V–1.25 V at 20 mV s^{-1} and 40 °C. Moreover, a linear sweep voltammogram (LSV) was recorded at BoT in a potential range of 1.25–1.65 V at 10 mV s^{-1} and 40 °C to determine the OER activity under CV conditions. During the chronoamperometric aging

test, the measured decay in current was found to lead to a small difference in Ohmic overpotential (BoT (61 A/g_{Ir}) ≈10 mV; EoT (33 A/g_{Ir}) ≈5 mV), therefore, no iR-compensation was required in this test.

Results and Discussion

Activity comparison of RDE and MEA measurements.—To identify the main reason for the remarkably different catalyst lifetimes estimated using MEA and RDE, we have employed a variety of OER catalyst durability testing procedures using a commercially available OER catalyst (IrO_2/TiO_2). As stability measurements require comparing applied potentials with corresponding currents or vice versa, it is important to confirm that both RDE and MEA measurements result in comparable OER activities. Therefore, the activities recorded from the two techniques were assessed.

Figure 1a shows the iridium mass-specific LSVs of the IrO_2/TiO_2 catalyst in the OER potential region for three RDE measurements (green lines) and two MEA measurements (blue circles and squares); Fig. 1b shows the corresponding Tafel plots. The results clearly indicate that within each technique, the measurements are quite reproducible. However, comparing the two techniques, the mass-specific OER activities obtained in RDE measurements are higher than those obtained in MEAs. This difference in activity may be explained either by the poor utilization of the catalyst in the MEAs, by the different loadings used in the two techniques, or by the effect of the ionomer content (Further details can be found in supplementary note A-1 available online at stacks.iop.org/JES/168/014512/mmedia). A poor utilization of the catalyst in the MEAs is excluded as the mass-specific capacitive currents of the MEAs (blue lines in Fig. 1c) are almost twice as large as the ones recorded in RDE experiments (green lines in Fig. 1c). A closer look shows that the polarization curve measured in MEA seems to be off by a constant value of ≈20 mV over a wide range of current density. Bernt et al.[40] showed that a local increase in partial pressure of oxygen at the electrode can lead to an additional loss in performance. The same holds true for an increase in partial pressure of hydrogen. By using a similar approach as Bernt et al., the 20 mV higher potential measured in MEA would equate to a difference in oxygen partial pressure of ≈10 bar or in hydrogen partial pressure of ≈2 bar ($\Delta p = p_{gas,cat} - p_{gas,channel}$). Although the values seem to be reasonable, Bernt et al. also showed a dependency on current density, which cannot be observed in this case. Hence, it is rather unlikely that an increase in partial pressure of oxygen and/or hydrogen within the catalyst layer is responsible for this discrepancy in activity.

It is, however, well known for platinum that high ionomer loadings can negatively impact the ORR activity[35] and thus the higher ionomer content used within the MEA configuration might explain the lower activity measured. As can be seen in figure A-1 within the supporting information the application of a higher ionomer content (20 wt.%) within the RDE configuration results in a significantly lower activity (≈3.5-times at 1.5 V_{RHE} (HFR-corrected)). Additionally, Bernt et al. showed that with increasing ionomer content, the activity is slightly decreasing.[39] Although no further studies were carried out to measure the change in activity as a function of ionomer content within the RDE configuration, we believe that the different ionomer contents used (1 wt.% ionomer in RDE measurements vs 11 wt.% in MEA measurements) are the origin of the discrepancy in OER activity measured by RDE and MEA. Nevertheless, the results obtained by both techniques are in reasonably good agreement; and therefore stability measurements were successfully assessed as shown in the next sections.

Chronopotentiometric (CP) aging test.—CP is the most frequently used method in the literature to estimate the stability of an OER catalyst by RDE measurements, where the observed increase in potential while applying a constant current is attributed to catalyst degradation, and ultimately to a complete loss of active material.[41–44] Figure 2a shows the potential transient recorded in

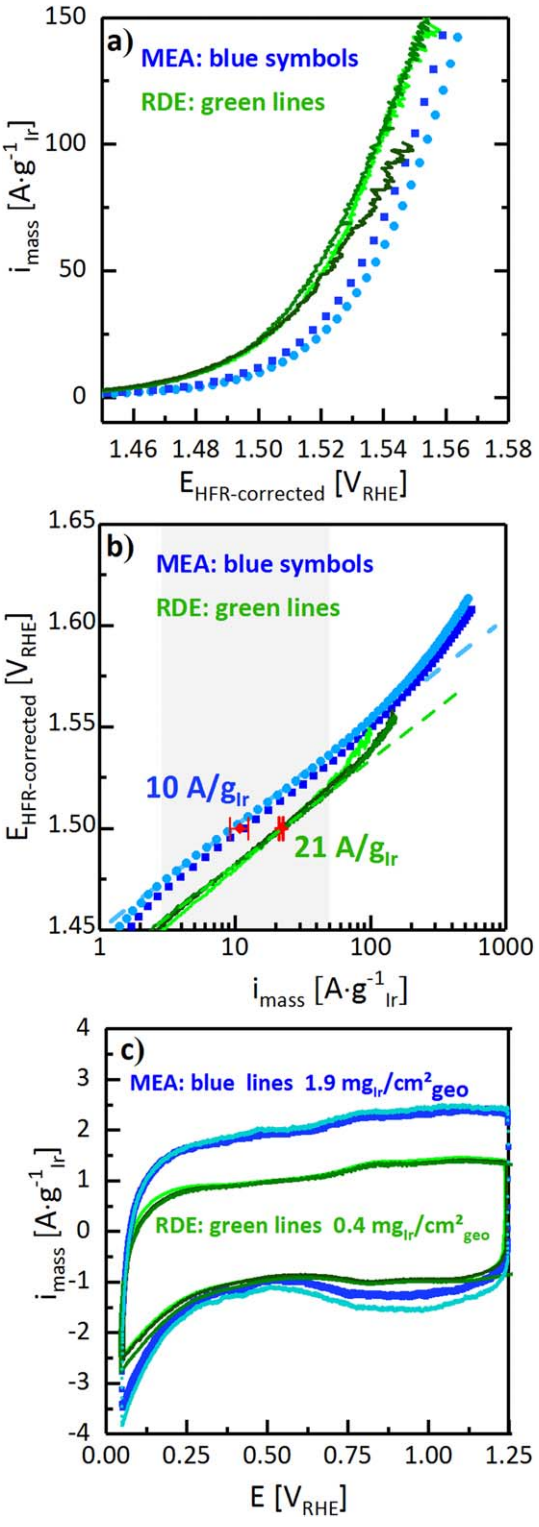

Figure 1. (a) Iridium mass-specific linear sweep voltammograms of the IrO_2/TiO_2 catalyst at 40 °C and 10 mV s^{-1} in MEAs (blue circles and squares) and in RDE experiments (green lines, 0.05 M H_2SO_4, Ar-saturated); (b) Tafel-plots (constructed from a) for three RDE measurements (green lines) and two MEA measurements (blue circles and squares), including the averaged activity determined at 1.50 V_{RHE} (HFR-corrected) indicated by the red symbols; (c) Cyclic voltammograms in the purely capacitive voltage region at 20 mV s^{-1} for three RDE measurements in Ar-saturated electrolyte (green lines) and for two MEA measurements with 50 nccm H_2 at the cathode side (blue lines).

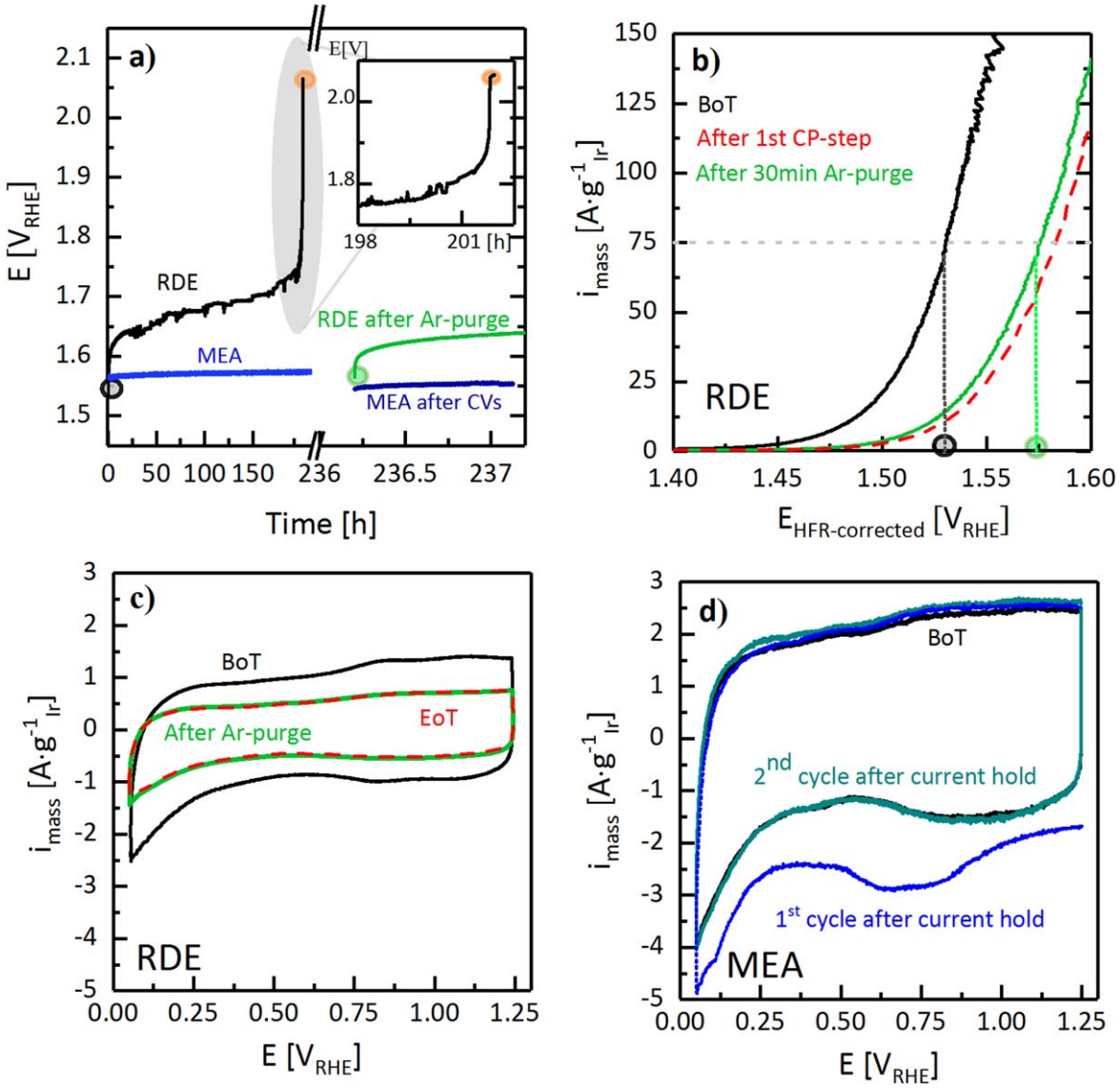

Figure 2. (a) Chronopotentiometry at 70 A g^{-1}_{Ir} of RDE measurements at BoT (black) and after purging with Ar for 30 min. (Ar-CV; 20 mVs^{-1}) (green curve) and MEA measurements at BoT (light blue) and after CV (50 nccm H_2 at the cathode) (dark blue). Inset shows the last hours of the first CP-step of the RDE measurements. (b) Mass-specific polarization curves for RDE measurements at BoT (black), after first CP-step and Ar-CV (green) and after second CP-step (EoT) and Ar-CV (red) recorded at 10 mV s^{-1}. (c) Cyclic voltammograms for RDE measurements recorded at BoT (black), after first CP-step (green) and after second CP-step (dotted red) at 20 mV s^{-1} in an Ar-purged electrolyte. (d) Cyclic voltammograms recorded for MEA measurements at BoT (black) and after first CP-step at 20 mV s^{-1}, where the first (blue) and the second (cyan) cycles after first CP-step are shown.

MEA and RDE measurements at a current density of 70 A g^{-1}_{Ir}. In the RDE experiment, the potential increases continuously (black line in Fig. 2a) reaching ≈1.75 V, at which a sudden potential jump occurs. Subsequently, the potential levels out at ≈2.1 V (orange circle, Fig. 2a inset), a potential one would measure when the same geometric current is applied to a bare Au-disk. [31] This behavior is typically interpreted in the literature by the degradation of the catalyst.[32,44] According to Eq. 1, an increase in OER overpotential (η) by one Tafel slope (TS; ca. 50 mV in this case) at a constant current (i), should correspond to a 90% loss of electrochemically active surface area or electrode roughness factor Ref. 31. Therefore, and according to this degradation hypothesis, no catalyst should remain after a total potential increase of >400 mV (black line in Fig. 2a).

$$\eta = TS \cdot \left[\lg\left(\frac{i}{i_0} \cdot \frac{1}{rf} \right) \right] \quad [1]$$

However, after the applied current was stopped and the electrolyte was purged with Ar for 30 min at 2500 rpm, followed by applying the same current (70 A g^{-1}_{Ir}), the starting potential of this second CP-step was almost the same as that that of the first CP-step, showing the same gradual increase of potential (green line in Fig. 2a). This result indicates that the catalyst did not collapse as suggested by the potential jump and that a correlation between this increase in potential and catalyst degradation seems highly unlikely. This increase in potential is related to an accumulation of microscopic oxygen bubbles and the concomitant shielding of active sites within the catalyst layer. [31] The formation and stability of such microscopic gas bubbles on the surface of gas evolving catalysts has been also shown by different imaging techniques such as total-internal reflection fluorescence (TIRF) microscopy, atomic force

microscopy (AFM) and X-ray radiography.[45–47] However, after the first CP-step was completed, the accumulated microscopic oxygen bubbles were removed by diffusion during the 30 min rotation in Ar-saturated electrolyte, which led to the re-exposure of active sites and performance recovery.

The potential increase was not detected in an MEA measurement in a PEM-WE, in fact, the performance was stable throughout the whole measurement period (~9 d) (light blue line in Fig. 2a). This drastic difference in the potential transient obtained in MEA vs RDE demonstrates that the RDE-based CP test cannot be reliably used to test the stability of OER catalysts.

After the initial CP-step with the MEA in the PEM-WE, OER polarization curves along with CVs are recorded and the same current is applied again (second CP-step, dark blue line Fig. 2a). Surprisingly, the initial potential of the second CP-step within the MEA configuration is even 10 mV smaller than that of the first CP-step and again showed a stable performance, a phenomenon observed elsewhere in literature, but never explained.[48] During operation, an increase in local partial pressure within the catalyst layer as well as the accumulation of oxygen bubbles is possible, however, distinguishing between the two is not trivial. The enhanced cell performance observed for the second CP-step within the MEA configuration might be related to either the microscopic oxygen bubbles formed and/or accumulated in the catalyst layer during the first CP-step or a developing local increase in oxygen and/or hydrogen partial pressure. Assuming that the increase in potential is only related to either an increase in partial pressure of oxygen or hydrogen, this would result in a pressure difference ($\Delta p = p_{gas,catalyst} — p_{gas,channel}$) of ≈2 bar and ≈0.5 bar respectively, both of the values being reasonable. While an increase in oxygen or hydrogen partial pressure can subside during OCV or zero current, the trapped oxygen bubbles can either be physically detached/diffuse away during the recorded CV under the water flow, or reduced electrochemically by scanning to low cathodic potentials (<1.0 V) within the MEA configuration. The latter is indicated by the additional cathodic current observed in the first CV (blue line in Fig. 2d) obtained after the first CP-step that is not observed in the second subsequent CV (cyan line in Fig. 2d).

To prove that the active sites are indeed shielded by microscopic oxygen bubbles, CVs and polarization curves were recorded for the RDE measurements subsequent to each CP-step and a 30 min. Ar purge. Figure 2b shows the mass-specific polarization curves recorded at the BoT (black line), after the first CP-step, a 30 min. Ar purge, and a subsequent CV (green line), and after the second CP-step, a 30 min Ar purge, and a subsequent CV (red dotted line). Quite nicely, the potentials corresponding to the 70 A g^{-1}_{Ir} in the polarization curves are in good agreement with the initial values of both CP-steps (black and green circles in Figs. 2a and 2b), proving that the polarization curves and the initial potentials of the CP measurements can indeed be correlated. According to Eq. 1, no catalyst should remain after the potential jump. However, the polarization curves reveal that there is still a sufficiently high OER activity compared to a bare Au-disk,[31] although significantly smaller compared to the initial activity. Accordingly, comparing the OER activities at 1.5 V_{RHE} suggests that only ≈20% of the initial catalyst layer seems to remain, whereas ≈80% is lost due to "microscopic bubbles-induced degradation." The accumulation of oxygen in the catalyst layer and partial shielding of the active sites result in an increasing potential at the remaining active sites to provide the same applied current. Consequently, the increased potential on the remaining active sites inevitably enhances iridium dissolution.[49–52] In fact, if the accumulation of microscopic bubbles could be avoided, no significant dissolution is expected to occur, since shielding a fraction of the catalyst layer is the main cause for the increasing potential and the accompanied iridium dissolution happening at the still accessible sites.

Figure 2c shows CVs measured at the BoT (black line), after the first CP-step (green line) and at EoT (red dotted line), each recorded after purging with Ar for 30 min to ensure a catalyst layer free of microscopic bubbles. The CVs recorded after the both CP-steps show that at least half of the initial catalyst layer is still electrochemically accessible. Conclusively, this comparison demonstrates that using chronopotentiometry for estimating the stability of an OER catalyst in RDE measurements is not reliable, since the observed increase in potential seems to be exclusively caused by the accumulation of microscopic oxygen bubbles and the by subsequent shielding of active sites within the catalyst layer.

Chronoamperometric (CA) aging test.—The observed decrease in current during a constant potential measurement is attributed to catalyst degradation and is commonly correlated to the lifetime of an OER catalyst.[14,29] In this study, a constant potential of 1.53 V_{RHE} (iR-corrected) is applied and the corresponding current is recorded during the RDE and MEA measurements. Within the first few minutes of a CA measurement in an RDE, a rapid decrease in the mass-normalized current of almost 75% can be observed (Fig. 3a, black curve), followed by a more gradual decrease in current over the subsequent 6 h. The initial OER activity of 56 A g^{-1}_{Ir} is taken after 100 ms, so that capacitive contributions are negligible (see experimental section). If this drop in current over the first hour were related to catalyst degradation, then almost 85% of the catalyst would have to be lost, even though this catalyst was proven to be stable in a PEM-WE over hundreds of hours.[17] Therefore, this rapid drop in current must be related to the fast filling of the catalyst layer with microscopic oxygen bubbles, shielding a significant fraction of the active sites, so that the current decreases.[31] Applying the same potential after purging for 30 min with Ar resulted in an initial current that is only 60% (34 A g^{-1}_{Ir}, green circle in Fig. 3a) of the initial current recorded for the first CA-step (gray circle in Fig. 3a), which again rapidly decays within the first hour of the second CA-step before it levels out (~ 5 A g^{-1}_{Ir}). While the rapid decay in current during the CA-step can undoubtedly be related to the partial shielding of active sites by microscopic oxygen bubbles, the 40% lower initial current in the subsequent second CA-step suggests that the catalyst also partially degraded during first CA-step. Polarization curves recorded at BoT, after the first CA-step, and at EoT, are provided at the supplementary note A-2.

Figure 3c shows that the CVs recorded after the first and second CA-steps (each preceded by a 30 min Ar purge) are ~30% smaller compared to the one measured at BoT (black curve in Fig. 3c), suggesting that roughly one third of the catalyst is degraded by the end of the experiment and that the decrease in current during a CA-step does not correlate to catalyst degradation. In summary, these results confirm that the stability of an OER catalyst cannot be examined by applying a constant potential in RDE measurements, since the current decrease is largely due to the shielding of active sites by microscopic oxygen bubbles, which are trapped in the catalyst layer.

Using the same catalyst in an MEA and testing it in a PEM-WE, it was found that the current decreased by ~50% after ~24 h (black curve in Fig. 3b), suggesting that half of the catalyst is either shielded or has degraded. The current at 1.53 V_{RHE} derived from a subsequently measured polarization curve after the first CA-step (33 A g^{-1}_{Ir}, purple star in Fig. 3b) closely matches the steady-state current (32 A g^{-1}_{Ir}) at 1.53 V_{RHE} after the 24 h CA-step. The current at 1.53 V_{RHE} also remains essentially constant (30 A g^{-1}_{Ir}) over a subsequent potential hold (dark blue curve in Fig. 3b), which either means that the catalyst has indeed degraded or that the O_2 bubbles are remaining in the catalyst layer.

Scanning the potential to below 1 V_{RHE} to remove the oxygen bubbles or to subside a local increase in oxygen and/or partial pressure in the catalyst layer, followed by a CA-step (turquoise curve in Fig. 3b), the same initial current at 1.53 $V_{RHE,HFR\text{-}corrected}$ (63 A g^{-1}_{Ir}) as that obtained for the first CA-step (61 A g^{-1}_{Ir}) was obtained. This firmly proves that the performance decay during a CA step was solely due to shielding the active sites by oxygen bubbles or the increase in local partial pressure of oxygen and/or hydrogen. An increase in partial pressure, however, would occur instantly and not

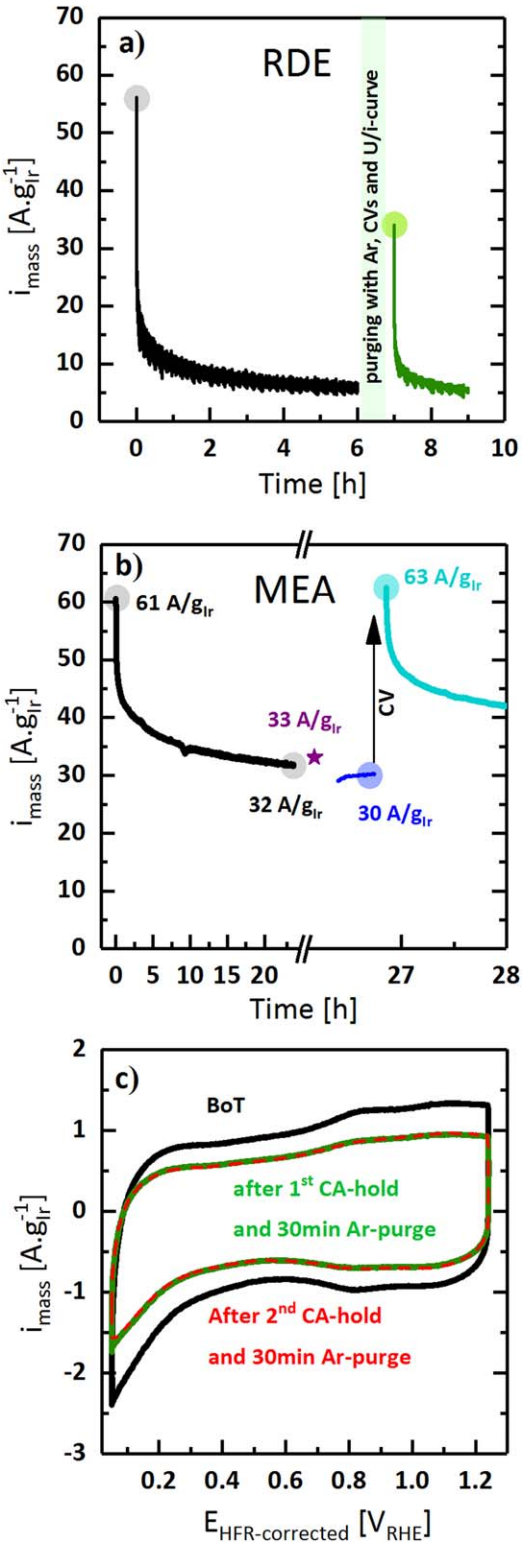

Figure 3. (a) Chronoamperometry at 1.53 V_{RHE} (internal iR-correction was applied) measured by RDE at BoT (black) and after first CA-hold (green). After each CA-hold, the electrolyte was purged with Ar for 30 min and a CV (see Fig. 3c) was recorded. (b) Chronoamperometry at 1.53 V_{RHE} (HFR-corrected) measured in an MEA at BoT (black), the purple star represents the activity measured at 1.53 V_{RHE} during a subsequent polarization curve, directly after the polarization curve (blue) and after a subsequent CV (turquoise). (c) Cyclic voltammograms recorded at BoT (black), after a 30 min. Ar-purge after the first CA-hold (green) and after a 30 min. Ar-purge after the second CA-hold at EoT (red dotted) at 20 mV s^{-1}.

over hours (see gradual decay in current over hours in Fig. 3b), wherefore an increase in partial pressure seems rather unlikely. So far, it is not trivial to give a solid explanation for whether this reversible degradation in an MEA is due to the electrochemical reduction of O_2, due to the removal of O_2 by diffusion, or an even more complex phenomenon.

Although the testing time in the MEA was much longer than that in the RDE configuration, no catalyst degradation was observed in the MEA, while for the RDE test, about 40% of the current could not be recovered. This confirms that using RDE measurements to predict the lifetime of a catalyst by applying a constant potential is not a valid approach, since the recorded drop in current is mostly due to the shielding of active sites by trapped microscopic oxygen bubbles and since the observed loss in OER activity is most likely a consequence of it. On the other hand, in MEA measurements, the current loss is reversible and it can be avoided by a proper design of the stability test.

Potential cycling aging test.—Undeniably, the OER catalyst stability during transient operation is of vital interest, since it will be an important consideration when coupling a PEM water electrolyzer with renewable energies that are inherently intermittent in power output.[53–56] By cycling the potential between idle periods (OCV) and times of operation (>1.4 V_{RHE}), the fluctuating power supply is commonly mimicked in RDE durability tests, and the observed decrease in OER activity is attributed to catalyst degradation.[5,7,14] In this study, the potential was cycled between 1.3 V_{RHE} and 1.6 V_{RHE}, avoiding reducing conditions, which can affect the performance of a PEM water electrolyzer.[17] Figure 4a depicts the mass-normalized current [A g^{-1}_{Ir}] extracted at 1.5 V_{RHE} from the anodic scan of the respective cycle during RDE measurements as a function of cycle number. Evidently, the current significantly drops within the first two cycles by ∼40% (cycles 1 and 2 in Fig. 4a), whereas the decrease slows down afterwards. After 20 cycles, only 40% of the initial activity is remaining (10 A g^{-1}_{Ir}, Fig. 4a), which means that 20 cycles would be enough to degrade more than half of the catalyst, assuming that this deactivation is owing only to catalyst degradation. However, after purging with Ar for 30 min and recording a CV, three additional cycles were performed (green circles in Fig. 4a), showing that roughly 70% of the initial activity can be recovered (∼15 A g^{-1}_{Ir}, red dotted circle). While a significant fraction of the catalyst degradation can be recovered, some irreversible catalyst degradation must have occurred, although this irreversible degradation is not expected in the here used potential range.[17,57] Again, the microscopic oxygen bubbles must be directly responsible for the reversible degradation, and indirectly responsible for the irreversible degradation.

The anodic scans of the individual cycles in the above RDE experiment are shown in Fig. 4c, where it becomes quite clear that the second cycle (dark green curve) during the first cycling test and the first one (red dotted line) recorded after a 30 min. Ar purge and a CV are perfectly identical, clearly demonstrating the partial recovery of activity. It can therefore be concluded that part of the catalyst layer degraded during the cycling test since only 70% of the current can be recovered by Ar purge. The CVs recorded for the potential cycling stability test at the BoT and at EoT are shown in Fig. A3.

The same stability protocol was executed in an MEA and the results are shown in Fig. 4b. Obviously, the current (∼12 A g^{-1}_{Ir}) recorded at 1.50 V_{RHE} during a polarization curve (purple diamond, measured galvanostatically beforehand) is similar to the current (∼12.5 A g^{-1}_{Ir}) obtained during the first anodic cycle at the same potential, whereas during the subsequent 200 cycles (light blue squares) the activity slightly decreases by ∼10%. This decrease is often interpreted in the literature as degradation of the catalyst,[5] however, after recording a polarization curve and a subsequent CV between 0.05–1.25 V_{RHE}, the activity increases to 16 A g^{-1}_{Ir} at 1.50 V_{RHE} (blue circles in Fig. 4b), i.e., to a value even higher than the one recorded during the very first cycle.

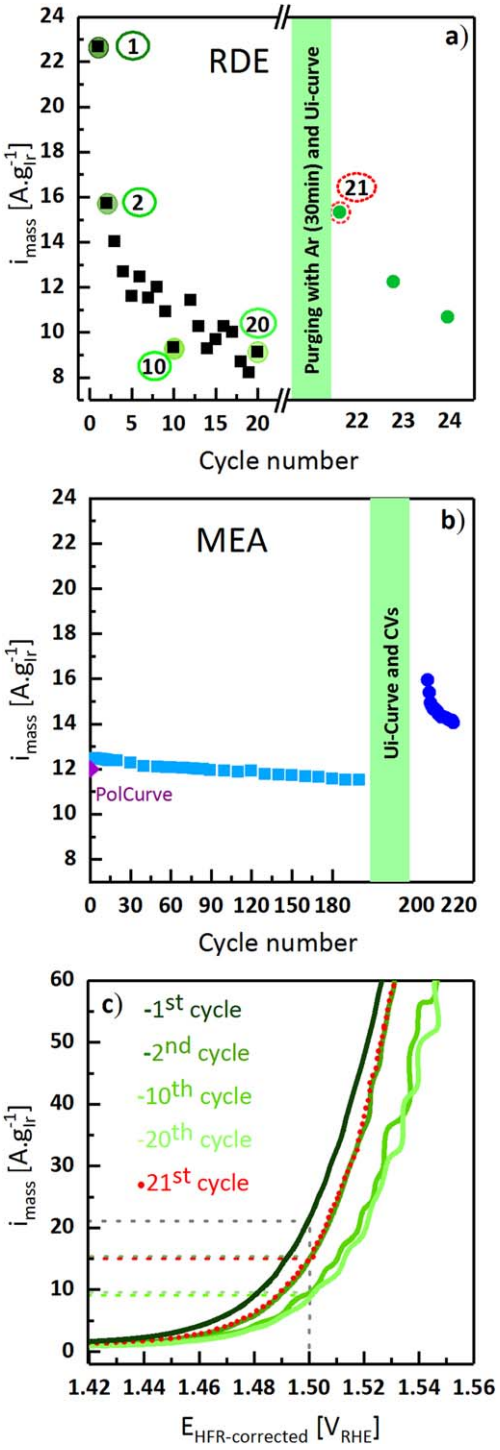

Figure 4. (a) Mass-specific currents, extracted at 1.50 V_{RHE} of the anodic scan during cycling between 1.3–1.60 V_{RHE} (iR-corrected) at 10 mV s^{-1} in RDE configuration, recorded for the initial 20 cycles (black squares) and for 3 cycles after a 30 min. Ar-purge, a CV and a polarization curve (green circles). (b) Mass-specific currents, extracted at 1.50 V_{RHE} during cycling between 1.3 V_{RHE}− 1.60 V_{RHE} (HFR-corrected) with 10 mV s^{-1} in an MEA, for the initial 200 cycles (light blue squares) and for 20 cycles (dark blue circles) recorded after obtaining a polarization curve and a CV. The purple diamond represents the extracted current at 1.50 V_{RHE} from the polarization curve recorded directly before the 200 cycles, and (c) Mass-specific anodic cycles (from RDE) recorded at 10 mV s^{-1} during cycling depicted for the first (dark green line), 2nd (green line), 10th (light green line), 20th (bright green line) and for the 22nd (red dotted line).

In contrast to the activity decrease over the course of the first 200 cycles, the decrease observed during the subsequent cycles is much more severe (−13% within 20 cycles). Both, the higher activity measured along with the observed fast decrease is related to the CV recorded directly before the second cycling, whereas the first cycling was recorded directly after measuring a polarization curve, during which large OER currents were drawn. By cycling the cell to lower cathodic potentials (<1.0 V_{RHE}), as it was already shown in the previous section (Fig. 2d), the microscopic oxygen bubbles trapped within the catalyst layer can be removed and/or an increase in oxygen and/or hydrogen partial pressure can decay. Since the cell was polarized at high potentials prior to the first cycling, a certain fraction of the catalyst layer must have already been shielded or a partial pressure difference was already developed and hence, did already affect the performance. This would explain the apparently lower activity along with the smaller decrease in activity during the first 200 cycles (light blue squares). On the other hand, once the catalyst layer is free of any microscopic oxygen bubbles after a CV into the potential range where O_2 can be reduced and any partial pressure buildup did subside, the catalyst can be fully utilized, which results in a high initial activity that, however, decays more rapidly due to the fast filling by microscopic oxygen bubbles and/or the increase in local partial pressure. In summary, this comparison shows that potential cycling cannot be used in RDE measurements to predict the lifetime of an OER catalyst, since the claimed degradation is caused by a shielding of active sites via trapped microscopic oxygen bubbles within the catalyst layer.

MEA aging for the three different aging protocols.—Each of the three investigated aging protocols showed that during MEA measurements in a PEM-WE, a fraction of the catalyst layer is shielded by microscopic oxygen bubbles and that by recording a CV to low potentials, the activity can be fully recovered. This suggests that there are no irreversible changes to the catalyst and the catalyst layer of the MEA during the test. Hence, the polarization curves recorded at BoT and at EoT should be identical, independent of which aging protocol is applied. The polarization curve representing the initial activity at BoT (black squares) and those recorded at the EoT for each aging protocol are depicted in Fig. 5a. In fact, the polarization curves at the end of the different stability tests match quite well with BoT performance, especially when the HFR-corrected curves are considered, thereby confirming that none of these aging tests caused any degradation of the catalyst and the catalyst layer. The corresponding HFRs as well as Tafel plots at BoT and at EoT are depicted in Fig. 5b. Further details regarding this figure can be found in supplementary note A-4.

We provide here a possible hypothesis (Fig. 6) as to why the effect of trapped oxygen bubbles is more pronounced in case of the RDE compared to MEA measurements. For this, we first focus on the processes occurring during MEA measurements in a PEM-WE. Since the through-plane electrical resistance within the catalyst layer is quite small (≈0.04 mΩ cm^2_{geo})[17] compared to the proton sheet resistance (14–30 mΩ cm^2_{geo}),[37] the OER reaction should mainly occur at the membrane/electrode interface (Fig. 6a).).[39] Thus, although the reaction is occurring throughout the whole catalyst layer, the utilization of the catalyst layer should be highest at the membrane/electrode interface. The catalyst layer thickness at a loading of 2 mg_{Ir} cm^{-2}_{geo} is ≈8–10 μm,[37] through which the produced oxygen has to escape. Within the OER catalyst layer, the local partial pressure of oxygen must thus increase, resulting in a pressure gradient from the membrane | electrode ($P_{O2,M|E}$) to the electrode | PTL interface ($P_{O2,E|PTL}$), illustrated by the blue curved line in Fig. 6a (marked as ①). This pressure difference might enhance the removal of oxygen within the catalyst layer towards the PTL, thereby minimizing the accumulation of oxygen within the catalyst layer.

The above consideration is only true, however, if a sufficiently large flux of water can be sustained from the electrode | PTL to the membrane | electrode interface. This, we believe, is provided by the

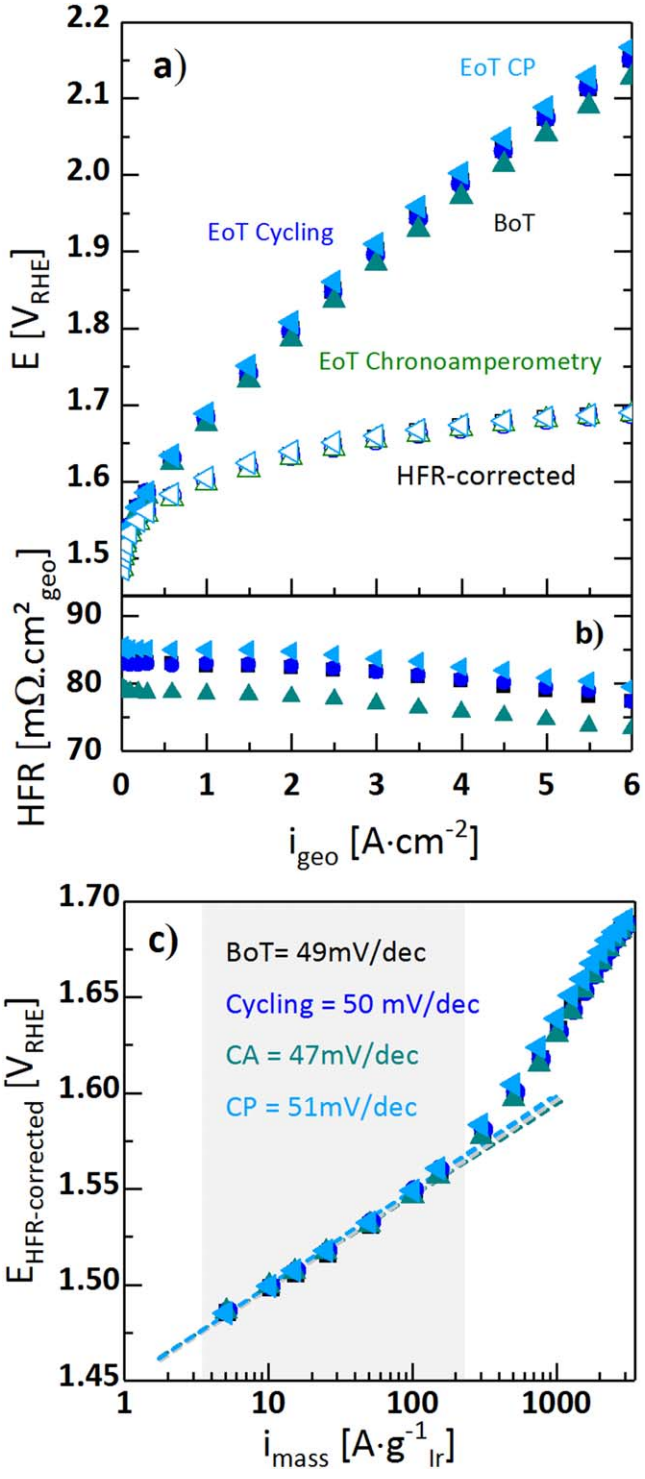

Figure 5. (a) Galvanostatically measured polarization curves at 40 °C recorded at BoT (black squares) and at EoT after 223 potential cycles between 1.3–1.60 V_{RHE} (blue circles), after ∼26 h of CA at 1.53 V_{RHE} (green triangles), and after ∼10 d of CP-hold at 70 A g^{-1}_{Ir} (light blue triangles); The open symbols represent the HFR-corrected polarization curves. (b) The corresponding HFRs as a function of current density. (c) Mass-specific Tafel-plots (data replotted from (a) at BoT (red line) and at EoT after 223 cycles (blue circles), after ∼26 h at 1.53 V_{RHE} (green triangles) and after ∼10 d at 70 A g^{-1}_{Ir} (light blue triangles). Please note that in many instances the data points overlap so closely that not all of the four different symbols can be discerned in each instance.

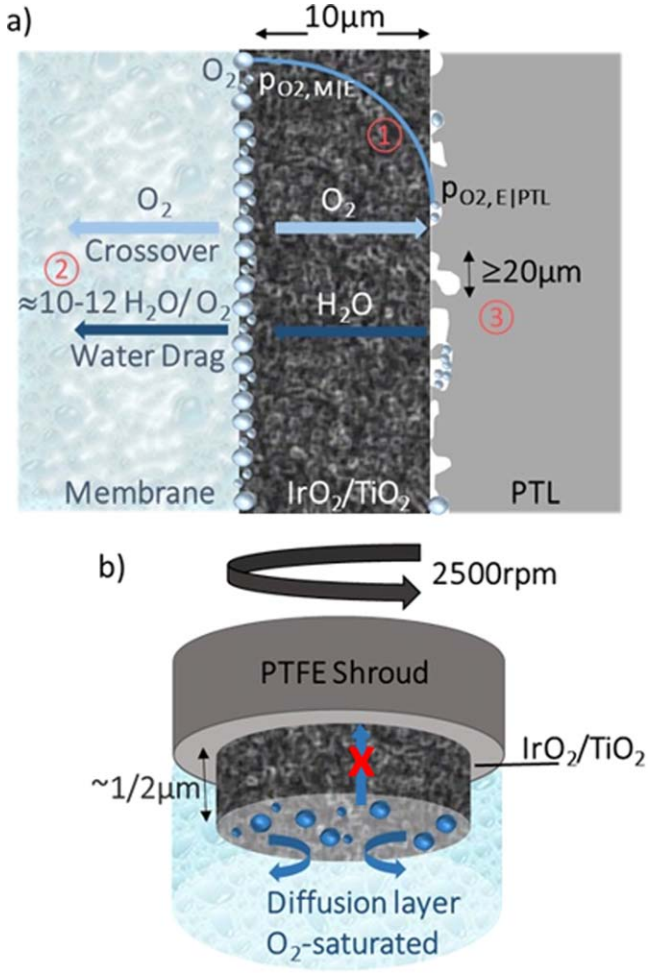

Figure 6. (a) Scheme of a single cell (MEA), illustrating possible reasons for a different degradation rate in MEA compared to an RDE: 1) pressure build-up within the catalyst layer; 2) electro-osmotic water drag and oxygen permeation; 3) restricting the size of a micro-bubble formed in an MEA | PTL interface to the pore diameter of the PTL. (b) Scheme of an RDE tip during OER operation.

electro-osmotic water drag from anode to cathode through the membrane (Fig. 6a, ②). The drag coefficient under electrolyzer operating conditions ranges between 2.5–3.2 H_2O/H^+, so that roughly 10–12 water molecules per produced oxygen molecule (4 H^+ per generated O_2) are dragged through the membrane and, consequently, through the anode catalyst layer, i.e., ≈5–6 times the amount required to produce one O_2 molecules.[58] This electro-osmotic water drag will thus sustain a sufficiently large flux of water to the membrane | electrode interface, so that the current density distribution across the anode catalyst layer will be governed by the proton conduction resistance. In this case, oxygen will be produced at a higher rate near the membrane | electrode interface (see above), producing the p_{O_2} gradient sketched by ① in Fig. 6a, which in turn allows for an efficient removal of O_2 gas bubbles from the anode catalyst layer. Additionally, the pore size of the PTL (⩾20 μm) may prevent the formation of macroscopic oxygen bubbles (0.1 −1 mm) and thus the blockage of larger sections of the anode catalyst layer (Fig. 6, ③). Commonly, however, a pressurized operation is desirable, while the whole study was conducted at ambient pressure. Bernt et al. showed that an increase in pressure leads to a higher hydrogen crossover.[59] Assuming the same holds true for oxygen crossover, an even more efficient removal of oxygen bubbles is expected for operations at higher pressure. Since there was already no degradation observed in the case of ambient pressure operation, none is expected in the case of pressurized operation.

On the other hand, in the RDE configuration, the oxygen can only be removed by diffusion within the catalyst layer or by convection in the radial direction at the outer surface of the catalyst layer (blue arrows, Fig. 6b) into an O_2-saturated electrolyte. Even in the absence of water transport resistances into the catalyst layer, the primary (i.e., conductivity-controlled) current distribution in this case favors the highest current density at the catalyst | electrolyte rather than at the disk | electrolyte interface, so no positive p_{O_2} gradient would be established from the disk | electrolyte to the catalyst | electrolyte interface to drive O_2 removal. In conclusion, the electro-osmotic drag of water across the catalyst layer of an MEA and the skewing of the OER current density distribution towards the membrane | electrode interface due a minimized proton conduction resistance are the most likely reason for the apparently more effective O_2 bubble removal in an MEA configuration. If one would be able to design a measurement setup, where one can stimulate dynamicity within the catalyst layer during the measurement in liquid electrolyte, one might be able to predict the lifetime of a catalyst without the need of an MEA setup. One possibility to prevent the accumulation of bubbles would be the application of sonication during operation,[33] which, however, is not feasible with catalyst in nano-particulate form. To the best of our knowledge, up to know there is no other technique other than assessing the long-term stability within in an MEA configuration, which can be used to reliably predict the lifetime of OER catalysts.

Conclusions

In this study, the most commonly used methods to predict the lifetime of OER catalysts, namely chronoamperometry, chronopotentiometry and potential cycling, were conducted in both RDE and MEA cells and directly compared with each other. It was demonstrated that none of the three investigated aging tests in an RDE configuration provides a measure of OER catalyst degradation/dissolution. This is mainly attributed to the accumulation of oxygen bubbles within the catalyst layer, shielding most of the active sites in case of an RDE test, resulting in a rapid increase in potential, for a CP test, or a rapid decrease in current, for a CA or potential cycling test, which is commonly interpreted as degradation of the catalyst. The accumulation of bubbles was found to induce irreversible degradation of the catalyst, a phenomenon that we did not observe in an MEA test. In fact, we demonstrated that while a local increase in partial pressure of oxygen and/or hydrogen seems rather unlikely, the accumulation of microscopic oxygen bubbles takes place also in an MEA, but to a much less extent compared to RDE. Therefore, the degradations observed in MEA for all the methods were fully reversible and almost no irreversible catalyst degradation was observed.

In summary, none of the most commonly used methods in RDE measurements is applicable to predict the lifetime of OER catalysts, since the observed decrease in performance is solely caused by the shielding of active sites via trapped microscopic oxygen bubbles. If it would be possible to prevent the accumulation of the microscopic oxygen bubbles within the catalyst layer during the measurement, it might be possible to design a proper stability protocol for testing OER catalysts using RDE measurements.

Acknowledgments

The authors gratefully acknowledge the German Ministry of Education and Research for financial support of this work within the Kopernikus project P2X (03SFK2V0) and the innoKA project (BMWi, 03ET6096A). The authors would like to thank Dr. Maximilian Bernt and Paulette Loichet (Chair of Technical Electrochemistry, Technical University of Munich, Germany) for fruitful scientific discussion.

Appendix

Supplementary information is available.

ORCID

Mohammad Fathi Tovini https://orcid.org/0000-0003-4334-4471
Hubert A. Gasteiger https://orcid.org/0000-0001-8199-8703

References

1. S. Cherevko, T. Reier, A. R. Zeradjanin, Z. Pawolek, P. Strasser, and K. J. J. Mayrhofer, *Electrochem. Commun.*, **48**, 81 (2014).
2. O. Kasian, S. Geiger, P. Stock, G. Polymeros, B. Breitbach, A. Savan, A. Ludwig, S. Cherevko, and K. J. J. Mayrhofer, *J. Electrochem. Soc.*, **163**, F3099 (2016).
3. Y. Lee, J. Suntivich, K. J. May, E. E. Perry, and Y. Shao-Horn, *J. Phys. Chem. Lett.*, **3**, 399 (2012).
4. P. Lettenmeier, L. Wang, U. Golla-Schindler, P. Gazdzicki, N. A. Cañas, M. Handl, R. Hiesgen, S. S. Hosseiny, A. S. Gago, and K. A. Friedrich, *Angewandte Chemie (International ed. in English)*, **55**, 742 (2016).
5. E. Oakton, D. Lebedev, M. Povia, D. F. Abbott, E. Fabbri, A. Fedorov, M. Nachtegaal, C. Copéret, and T. J. Schmidt, *ACS Catal.*, **7**, 2346 (2017).
6. H. Ohno, S. Nohara, K. Kakinuma, M. Uchida, A. Miyake, S. Deki, and H. Uchida, *J. Electrochem. Soc.*, **164**, F944 (2017).
7. T. Reier, M. Oezaslan, and P. Strasser, *ACS Catal.*, **2**, 1765 (2012).
8. S. Zhao, A. Stocks, B. Rasimick, K. More, and H. Xu, *J. Electrochem. Soc.*, **165**, F82 (2018).
9. N. H. Kwon, M. Kim, X. Jin, J. Lim, I. Y. Kim, N.-S. Lee, H. Kim, and S.-J. Hwang, *NPG Asia Mater.*, **10**, 659 (2018).
10. Y.-T. Kim et al., *Nat. Commun.*, **8**, 1449 (2017).
11. S. Geiger, O. Kasian, A. M. Mingers, S. S. Nicley, K. Haenen, K. J. J. Mayrhofer, and S. Cherevko, *ChemSusChem*, **10**, 4140 (2017).
12. K. E. Ayers, E. B. Anderson, K. Dreier, and K. W. Harrison, *ECS Trans.*, **50**, 35 (2013).
13. C. Rakousky, U. Reimer, K. Wippermann, M. Carmo, W. Lueke, and D. Stolten, *J. Power Sources*, **326**, 120 (2016).
14. S. M. Alia, B. Rasimick, C. Ngo, K. C. Neyerlin, S. S. Kocha, S. Pylypenko, H. Xu, and B. S. Pivovar, *J. Electrochem. Soc.*, **163**, F3105 (2016).
15. H.-S. Oh, H. N. Nong, T. Reier, A. Bergmann, M. Gliech, J. Ferreira de Araújo, E. Willinger, R. Schlögl, D. Teschner, and P. Strasser, *JACS*, **138**, 12552 (2016).
16. S. Geiger et al., *Nat. Catal.*, **1**, 508 (2018).
17. A. Weiß, A. Siebel, M. Bernt, T.-H. Shen, V. Tileli, and H. A. Gasteiger, *J. Electrochem. Soc.*, **166**, F487 (2019).
18. C. Spöri, J. T. H. Kwan, A. Bonakdarpour, D. P. Wilkinson, and P. Strasser, *Angewandte Chemie (International ed. in English)*, **56**, 5994 (2017).
19. C. C. L. McCrory, S. Jung, J. C. Peters, and T. F. Jaramillo, *JACS*, **135**, 16977 (2013).
20. B. S. Yeo, *Nat. Catal.*, **2**, 284 (2019).
21. Y. Yao et al., *Nat. Catal.*, **2**, 304 (2019).
22. Y. Lin, Z. Tian, L. Zhang, J. Ma, Z. Jiang, B. J. Deibert, R. Ge, and L. Chen, *Nat. Commun.*, **10**, 162 (2019).
23. J. Guan, Z. Duan, F. Zhang, S. D. Kelly, R. Si, M. Dupuis, Q. Huang, J. Q. Chen, C. Tang, and C. Li, *Nat. Catal.*, **1**, 870 (2018).
24. J. Wang, L. Han, B. Huang, Q. Shao, H. L. Xin, and X. Huang, *Nat. Commun.*, **10**, 5692 (2019).
25. L. Cao et al., *Nat. Commun.*, **10**, 4849 (2019).
26. F. Shi, Z. Geng, K. Huang, Q. Liang, Y. Zhang, Y. Sun, J. Cao, and S. Feng, *Advanced science (Weinheim, Baden-Wurttemberg, Germany)*, **5**, 1800575 (2018).
27. J. Kim, P.-C. Shih, K.-C. Tsao, Y.-T. Pan, X. Yin, C.-J. Sun, and H. Yang, *JACS*, **139**, 12076 (2017).
28. M. Tahir et al., *ACS Energy Lett.*, **2**, 2177 (2017).
29. Y. Wu, W. Sun, Z. Zhou, W. Q. Zaman, M. Tariq, L. Cao, and J. Yang, *ACS Omega*, **3**, 2902 (2018).
30. M. Bernt, A. Weiß, M. F. Tovini, H. A. El-Sayed, C. Schramm, J. Schröter, M. Kemmer, C. Gebauer, and H. A. Gasteiger, *Chem. Ing. Tech.*, **92**, 31 (2020).
31. A. W. H. A. El-Sayed, L. F. Olbrich, G. P. Putro, and H. A. Gasteiger, *J. Electrochem. Soc.*, **166**, F1 (2019).
32. X. Tan, J. Shen, N. Semagina, and M. Secanell, *J. Catal.*, **371**, 57 (2019).
33. A. Hartig-Weiss, M. F. Tovini, H. A. Gasteiger, and H. A. El-Sayed, *ACS Appl. Energy Mater.*, **3**, 10323 (2020).
34. B. G. Pollet, F. Foroughi, A. Y. Faid, D. R. Emberson, and M. H. Islam, *Ultrason. Sonochem.*, **69**, 105238 (2020).
35. K. Shinozaki, J. W. Zack, S. Pylypenko, B. S. Pivovar, and S. S. Kocha, *J. Electrochem. Soc.*, **162**, f1384 (2015).
36. M. Bernt, A. Hartig-Weiß, M. F. Tovini, H. A. El-Sayed, C. Schramm, J. Schröter, C. Gebauer, and H. A. Gasteiger, *Chem. Ing. Tech.*, **92**, 31 (2020).
37. M. Bernt, A. Siebel, and H. A. Gasteiger, *J. Electrochem. Soc.*, **165**, F305 (2018).
38. M. Carmo, D. L. Fritz, J. Mergel, and D. Stolten, *Int. J. Hydrogen Energy*, **38**, 4901 (2013).
39. M. Bernt and H. A. Gasteiger, *J. Electrochem. Soc.*, **163**, F3179 (2016).
40. M. Bernt and H. A. Gasteiger, *J. Electrochem. Soc.*, **163**, F3179 (2016).
41. O. Diaz-Morales, S. Raaijman, R. Kortlever, P. J. Kooyman, T. Wezendonk, J. Gascon, W. T. Fu, and M. T. M. Koper, *Nat. Commun.*, **7**, 12363 (2016).
42. L. Yang et al., *Nat. Commun.*, **9**, 5236 (2018).
43. C. Yang et al., *Nat. Commun.*, **11**, 1378 (2020).
44. H.-S. Oh, H. N. Nong, T. Reier, M. Gliech, and P. Strasser, *Chem. Sci.*, **6**, 3321 (2015).
45. E. Leonard, A. D. Shum, S. Normile, D. C. Sabarirajan, D. G. Yared, X. Xiao, and I. V. Zenyuk, *Electrochim. Acta*, **276**, 424 (2018).

46. L. Zhang, Y. Zhang, X. Zhang, Z. Li, G. Shen, M. Ye, C. Fan, H. Fang, and J. Hu, *Langmuir*, **22**, 8109 (2006).
47. R. Hao, Y. Fan, M. D. Howard, J. C. Vaughan, and B. Zhang, *Proc. Natl Acad. Sci.*, **115**, 5878 (2018).
48. A. S. Aricò, S. Siracusano, N. Briguglio, V. Baglio, A. Di Blasi, and V. Antonucci, *J. Appl. Electrochem.*, **43**, 107 (2013).
49. S. M. Alia and G. C. Anderson, *J. Electrochem. Soc.*, **166**, F282 (2019).
50. O. Kasian, J.-P. Grote, S. Geiger, S. Cherevko, and K. J. J. Mayrhofer, *Angewandte Chemie (International ed. in English)*, **57**, 2488 (2018).
51. D. N. Buckley and L. D. Burke, *J. Chem. Soc., Faraday Trans. 1 F*, **71**, 1447 (1975).
52. M. Pourbaix, *Atlas of Electrochemical Equilibria in Aqueous Solutions* (NACE International, Houston Texas, United States of America) 2nd edn. ed. (1974).
53. F. Barbir, *Sol. Energy*, **78**, 661 (2005).
54. R. E. Clarke, S. Giddey, F. T. Ciacchi, S. P. S. Badwal, B. Paul, and J. Andrews, *Int. J. Hydrogen Energy*, **34**, 2531 (2009).
55. C. Rakousky, U. Reimer, K. Wippermann, S. Kuhri, M. Carmo, W. Lueke, and D. Stolten, *J. Power Sources*, **342**, 38 (2017).
56. A. Buttler and H. Spliethoff, *Renew. Sustain. Energy Rev.*, **82**, 2440 (2018).
57. S. Cherevko, S. Geiger, O. Kasian, A. Mingers, and K. J. J. Mayrhofer, *J. Electroanal. Chem.*, **773**, 69 (2016).
58. W. Vielstich, A. Lamm, H. A. Gasteiger, and H. Yokokawa (ed.), *Handbook of Fuel Cells: Perfluorinated Membranes* (John Wiley & Sons, Ltd., Chichester, United Kingdom) (2010).
59. M. Bernt, J. Schröter, M. Möckl, and H. A. Gasteiger, *J. Electrochem. Soc.*, **167**, 124502 (2020).